Applied Ocean Research 86 (2019) 73–86

Contents lists available at ScienceDirect

Applied Ocean Research

journal homepage: www.elsevier.com/locate/apor

Rayleigh-Ritz method-based analysis of dry coupled horizontal-torsional-warping vibration of rectelliptic open-section containership bare-hulls

J.D. Thekinen[a], N. Datta[b,*]

[a] Department of Mechanical Engineering, Purdue University, West Lafayette, USA
[b] Indian Institute of Technology, Kharagpur, India

ARTICLE INFO

Keywords:
Hull girder vibration
Open section
Arbitrary distribution
Rectellipse
Rayleigh-Ritz method
Modal convergence

ABSTRACT

The coupled horizontal-torsional-warping vibration of a thin-walled open-section 7800 TEU container ship bare-hull, modelled as a non-uniform girder, is analysed by the efficient energy-based Rayleigh-Ritz method, in order to generate the dry asymmetric vibration frequencies. Since the centre of gravity is within the hull and the shear centre is below the keel, the horizontal and torsional modes of vibration are highly coupled. An open section is also prone to warping. In a novel attempt, the bare-hull geometry is generated mathematically, using section-wise closed-form semi super-ellipses (Lame's curves). The main dimensions, weight distributions, and fineness ratios are preserved, and closed-form expressions of sectional properties become available in the process. The hull has arbitrarily (non-mathematically) varying mass, bending stiffness, warping stiffness, and shear stiffness distributions along the length. The non-uniform beam modeshape in horizontal/torsional vibration is assumed to be a weighted sum of the uniform beam horizontal/torsional modeshapes. Several benchmark cases of simpler geometry have been analysed first, for both torsion-warping vibration, and coupled horizontal-torsional-warping vibration. Pontoon approximation of the containership has been analysed and validated. Subsequently, the coupled dry vibration frequencies are obtained for the open deck non-uniform girder, and compared with published results.

1. Introduction

Ocean going cargo vessels, by virtue of being large and long, are subject to significant dynamic stresses due to environmental forces and internal machinery. The investigation of the vibratory stresses is crucial for the safe design of marine structures. Global, steady-state, lightly damped, lower frequency-higher amplitude vibration of the ship hull girder is called springing, which may result in global shear stresses and fatigue. The fundamental frequency of hull girder vibration should be avoided at all encounter speeds. Thus, the estimation of the natural frequencies forms an integral part of the structural design.

Foropen-section container ships, a major structural design concern is torsional flexure (including warping), which leads to high shear stresses, especially in oblique seas. In modern times, large container ships may go up to 400 m in length and 60 m in beam. The hatch opening is as large as the beam itself, which adversely affects the torsional rigidity of the vessel. Open-section container ships are subjected to torsional moments in the quartering sea conditions. With the vessel heading obliquely into the waves, there are opposing exciting moments fore and aft of the vessel, leading to torsion-warping. There are large horizontal bending moments in quartering and beam seas, leading to horizontal springing. Containerships are open-section hull-forms, causing the shear centre to lie much beneath its keel line. Additionally, stacking of containers above the deck causes the centre of gravity to rise in the loaded condition. This results in a large offset between the centre of gravity and the shear centre, called 'eccentricity', which causes significant coupling between the horizontal and torsional vibration modes.

The premise of this work is as follows:

- The containership hull is open-section, with a single plane of symmetry (port and starboard). The large gap between the centre of gravity and shear centre causes a strong coupling between the horizontal and torsional modes of vibration.
- The thin-walled open-section hull undergoes warping in the coupled horizontal-torsional vibration. As shown by Li et al. [1], the length-to-depth must be at least 70 in order to ignore warping. In our case study here (7800TEU container, Senjanović 2009), the length-to-breadth ratio is 7.80, and the length-to-depth ratio is 13.6. For this slenderness ratio, warping may lead to a 2–2.5 times increase in the pure-torsional frequencies; and thus cannot be ignored.

* Corresponding author at: Department of Ocean Engineering and Naval Architecture, Indian Institute of Technology, Kharagpur, India.
E-mail address: nabanitadatta@gmail.com (N. Datta).

https://doi.org/10.1016/j.apor.2019.01.032
Received 21 October 2017; Received in revised form 6 January 2019; Accepted 29 January 2019
Available online 28 February 2019

Nomenclature

E	Modulus of elasticity of the material
G	Shear modulus of the material
ρ	Density of the material
x	Independent space variable along the length of the vessel (Positive from AP to FP)
$\boldsymbol{y}(x, z)$	Vessel offset along the breadth of the vessel (Positive towards starboard)
z	Independent space variable along the depth of the vessel (Positive upwards)
t	Independent time variable
$\Psi(x, y)$	Warping function
$\boldsymbol{\Theta}(x, t)$	Angle of twist of the non-uniform cross section in torsional vibration
$\theta(x, t)$	Angle of twist of the uniform cross section in torsional vibration
$Z_H(x, t)$	Flexural displacement in horizontal vibration
$Z_V(x, t)$	Vertical vibratory displacement
$\Theta_j(x)$	jth non-uniform torsional mode
$\theta_j(x)$	jth uniform beam torsional mode
$\Phi_j(x)$	jth non-uniform beam flexural mode
$\varphi_j(x)$	jth uniform beam flexural mode
$I_p(x)$	Polar moment of area of cross section
$I_w(x)$	Warping constant
$J(x)$	Torsion constant
$c(x)$	Distance between centre of gravity and shear centre
$I_{bv}(x)$	Second moment of area about horizontal neutral axis
$I_{bh}(x)$	Second moment of area about vertical neutral axis
γ_j	Frequency parameter of the jth uniform beam modeshape
T	Total kinetic energy of the beam
U	Total potential energy of the beam

- The sectional mass and stiffness properties vary *arbitrarily* along the length : there is no mathematical function to define them. Thus, closed-form analytical solutions to vibration energies, frequencies, and modeshapes are not possible.
- The ends are free, i.e. free to translate, rotate, twist, warp. The shear force and the bending moment are zero at the ends. The total torque (twisting + warping) is zero at the free end, and the warping bi-moment is also zero.
- The dry frequencies of torsional vibration coupled with horizontal vibration, including warping, are to be calculated. Uncoupled modes over-predict the frequencies, falsely assuring low chances of resonance with waves.
- The coupled horizontal-torsional-warping non-uniform modeshapes are obtained through this work, and they act as inputs in the mode-superposition method for the hydroelastic analysis of the vessel under wave-induced flexure.

1.1. Literature review : torsional vibration of uniform and non-uniform beams

Pouyet and Lataillade [2] studied the torsional vibration of non-uniform shafts ignoring warping. The work was limited to *mathematical variations* of the cross-section, leading to closed-form solutions of the torsional modeshapes and frequencies. Dokumaci [3] introduced a method of frequency-search to study coupled torsion-horizontal vibration, ignoring warping. Rao and Mirza [4] studied free torsional vibration, including effects of warping, through Galerkin's finite element method : however the analysis was limited to *linearly tapered* cantilever beams. The shape functions were third-degree polynomials for the angle of twist, and the Eigen vectors and torsional modeshapes were not investigated. Bishop et al. [5] extended the method introduced by Dokumaci [3] to study coupled torsion-warping-horizontal vibration for *uniform* (prismatic) beams by the frequency search method. It established the huge errors in torsional frequencies if warping was excluded, even in closed-section uniform beams. Li et al [1] studies the torsion-warping vibration of uniform I-section beams, uncoupled from horizontal vibrations. Also, the free-edge conditions used were approximate and did not account for the total twisting torque including warping to be zero at the ends. Eisenberger [6] studied torsional vibration of tapered beams including the effects of warping, with *polynomial* variation of sectional properties, approximate boundary conditions, and the modeshapes assumed as an infinite power series. However, the methodology still required solution for a large number of simultaneous equations. Sapountzakis [7] studied the *static* torsion of various non-uniform cross-sections with boundary element method. This work was continued in Sapountzakis and Mokos [8].

1.2. Literature review : anti-symmetric hull girder vibration

Bishop and Price [9], in their pioneering book on ship hydroelasticity, discuss the basic analysis methodology of anti-symmetric (horizontal and torsional) vibration of ships, including shear deformation and warping. However, four decades ago, no real-time results were available for the dry and wet natural frequencies of coupled horizontal-torsional warping vibration of ships. Pedersen [10] used 1D FEA model to study the torsion-warping vibrations of a prismatic thin-walled hull. Senjanovic [11–15] has done an extensive and comprehensive analysis of the torsion-warping-longitudinal coupled vibration of open-section thin-walled ship-like girders. However, Finite Element Method was the major methodology of analysis and admissible function for uniform beams. Senjanović and Ćatipović [13] used the energy-based method to solve the differential equations for the coupled horizontal-torsional-warping vibration, but the girder was uniform (prismatic) and torsion-warping boundary conditions were simplified. Also, separate formulations were done for vertical/torsional modeshapes symmetric and anti-symmetric about midships, increasing theoretical calculations.

1.3. Overview of this work

For global vibration analysis, the hull girder is modelled as a non-uniform Euler-Bernoulli beam. The sectional properties (mass and stiffness distributions along the length of the hull) have no mathematical/analytical expressions, which *could have* led to closed-form expressions for the potential and kinetic energies of the beam. At each section (station), the sectional shape (visible in the body plan) again has no mathematical expression, which *could have* led to closed-form expressions for sectional mass and stiffness. Now suppose there *was* a closed-form expression of a section shape, the accuracy of the sectional properties thus calculated would be highly enhanced. However, the hull section resembles none of the known geometric shapes known, e.g. circle, ellipse, parabola, polygon, etc. A non-mathematical function requires numerical integration. This work overcomes the disadvantage of lack of mathematical geometry definitions : the concept of rectellipse (rectangle + ellipse, i.e. a shape in between a rectangle and an ellipse), a superset of Lame's curves, is very versatile in replicating most of the hull section shapes. Using them to generate the ship hull body-plan gives closed-form expressions for sectional properties. This leads to an accurate length-wise mass and stiffness distributions, and improves the accuracy of the energy calculations, leading to more reliable estimates of hull girder frequencies.

In the present work, a merchant ship hull (7800TEU containership) is modelled mathematically with semi-superellipses, replicating a major part of the standard body plan. The mathematical and NURBS body plan are blended together to form a hybrid body plan. The main dimensions and fineness ratios (block coefficient C_b, prismatic coefficient C_p, midship section area coefficient C_M, water plane-area coefficient C_{wp}) of the ship are retained in the process. The closed-form expressions for the sectional properties are easily calculated, leading superior estimates of the potential and kinetic energies. First, the vertical-plane vibration frequencies are generated by the Rayleigh-Ritz method, using the admissible function as a series summation of the uniform beam modeshapes (admissible functions); as detailed by Datta and Thekinen [16]. The same energy-based approach is used to analyse horizontal/torsional vibration of the non-uniform beam, including warping. The coupled horizontal/torsional/warping frequencies are generated for the open deck non-uniform girder. Comparative studies are made by Finite Element Method to justify the validity of the present method. The novelty of the work lies in the following:

1 *Use of rect-ellipses to model and analyse a mathematical hull.* In previous works, structural dynamics and hydrodynamic added mass and damping are calculated only for Non-Uniform Rational B-Spline (NURBS) surfaces or Lewis sections. In the present work, the same is achieved for a 3D body with semi-super-elliptic sections (*see* Section 2).
2 *Use of Rayleigh-Ritz method to analyse the natural frequencies of vibration of a hull girder with non-prismatic cross-section.* In most of the previous published work, hull vibration has been studied using Finite Element Analysis (FEA). In present study the results are obtained by the Rayleigh-Ritz (R—R) method are then verified by comparative studies using FEA. The computational supremacy of the Rayleigh-Ritz method with reasonable accuracy over FEA is justified.
3 *Use of accurate torsional-warping boundary conditions.* For a free-free hull girder, the boundary conditions have been modelled fully, which have been approximated in earlier literature. This leads to accurate uniform torsion-warping modeshapes, which are used in the Rayleigh-Ritz method to establish the non-prismatic hull girder vibration.

2. Superellipse

The range of typical ship sections that can be generated by a semi-rectellipse, and its application to model hull sections has been detailed in this section (previously shown in Datta and Thekinen [17]). A rect-ellipse follows the equation

$$\left(\frac{\mathbf{y}(x,z)}{a(x)}\right)^{p(x)} + \left(\frac{z}{b(x)}\right)^{q(x)} = 1 \tag{1}$$

Here, z is the waterline measured from the main deck, and $\mathbf{y}(x, z)$ is the hull offset measured from the centreline, which is a function of two independent variables, i.e. (i) the station x and (ii) the waterline z. A semi-rectellipse requires four positive parameters to define itself, viz. $a(x)$, $b(x)$, $p(x)$, $q(x)$. The parameters $a(x)$ and $b(x)$ are the semi-major and semi-minor axes of the rectellipses, respectively. The powers $p(x)$ and $q(x)$ determine the shape of the curve. Curve-fitting and assumptions based on the general shape of semi-rectellipse are used to identify $p(x)$ and $q(x)$. Adjusting these parameters leads to the generation of a very wide range of shapes; and the typical ship sections are a subset of this range. If $p(x)$ and $q(x)$ are greater than 2, we get a super-ellipse. If they are equal to 2, we get back the well-known ellipse. If they are less than 2, we get sub-ellipses. Fig. 1(a,b,c) shows the geometrical shapes traced by a semi-rectellipse for 3 broad categories of parameters. For Fig. 1(a), both p and q are greater than 2, which leads to a *full-form* shape. For Fig. 1(b), p is greater than 2, q is less than 2 to bring in a *flare* shape. In Fig. 1(c), p is less than 2 and q is greater than 2 to generate a *stern overhang* section shape.

- Fig. 2(a) : As $p, q \to \infty$, the bilge radius → 0 and the sections become more squarish, and corners sharper.
- Fig. 2(b) : As $p \to \infty\,(p > 2)$ and $q \to 0\,(q < 2)$, the keel plate breadth → moulded breadth, and flares get manifested.
- Fig. 2(c) : As $p \to 0\,(p < 2)$ and $q \to \infty\,(q > 2)$, the deadrise angle → 0, without compromising on the beam B.
- Order p, $q = 1$ gives a wedge section.

On varying the parameters of the super-ellipse it is conveniently generating typical midship section (large values of p and q), forward flare (fractional values of q) and propeller stern overhang sections (fractional values of p).

2.1. Methodology of application of semi-superellipse to generate the hull section shape

To define a section of the hull girder and replicate the body plan as closely as possible, we require four (4) parameters as inputs ($a(x)$, $b(x)$, $p(x)$ and $q(x)$), as mentioned in Eq. (1). The semi-major and semi-minor axes at each station $a(x)$ and $b(x)$ are exactly same as the local half-

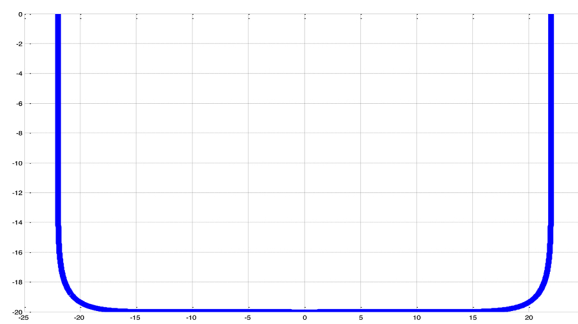

(a) Midship Section, $a = 22$, $b = 20$, $p = 12$, $q = 12$

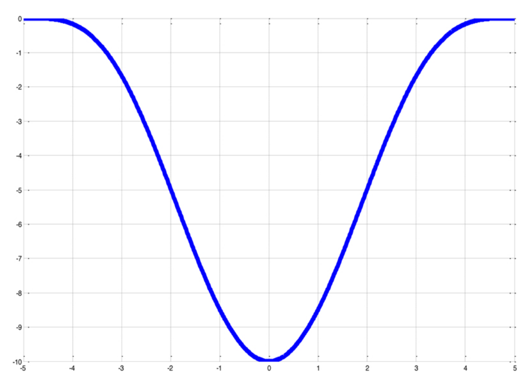

(b) Forward Section, $a = 5$, $b = 10$, $p = 2$, $q = ¼$

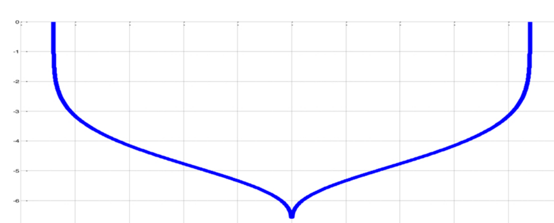

(c) Stern section, $a = 22$, $b = 7$, $p = 1/5$, $q = 5$

Fig. 1. (a) Midship Section, $a = 22$, $b = 20$, $p = 12$, $q = 12$. (b) Forward Section, $a = 5$, $b = 10$, $p = 2$, $q = ¼$. (c) Stern section, $a = 22$, $b = 7$, $p = \frac{1}{5}$, $q = 5$.

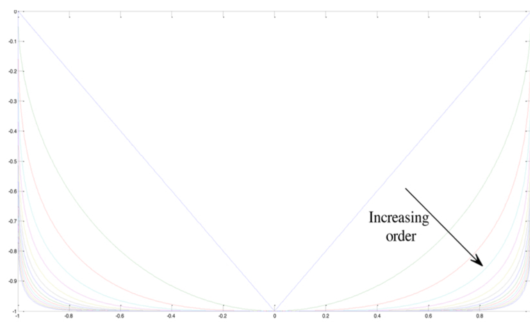

(a) Midship Section $(p, q \rightarrow \infty)$

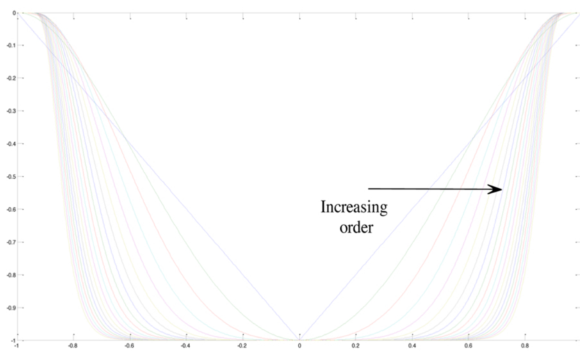

(b) Forward section $(p \rightarrow \infty,\ q \rightarrow 0)$

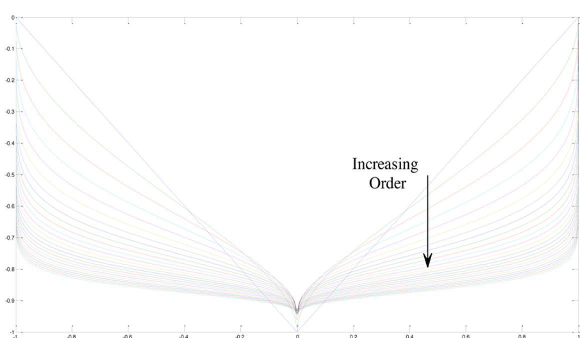

(c) Stern section $(p \rightarrow 0,\ q \rightarrow \infty)$

Fig. 2. (a) Midship Section $(p,\ q \rightarrow \infty)$. (b) Forward section $(p \rightarrow \infty,\ q \rightarrow 0)$. (c) Stern section $(p \rightarrow 0,\ q \rightarrow \infty)$.

breadth and depth respectively. The range of values, that need to be chosen for $p(x)$ and $q(x)$ in order to generate the typical sections along the length of the hull, is identified above. Based on these assumptions, by curve-fitting, any section can be replicated and optimized values of p and q are identified. A MATLAB program is developed to follow the procedure for any number of stations; and a major length of the hull (if not the total length of the hull) can be replaced by a collection of semi-rectellipses. It is important to note that while the semi-rectellipse can conveniently generate forward flare, sections amidships and stern overhang; sections extreme aft and extreme fore (like bulbous bow etc.) cannot be generated. Hence the final body plan will be a blend of semi-superelliptic sections and B-spline sections. NURBS (Non-uniform rational B-Spline) surfaces can be suitably employed for the hull form design. Once the basic design is obtained, the body plan can be imported into an image-reading code in MATLAB which can replace a wide range of body plan sections with equivalent semi-rectellipses. The subsequent hull form can be conveniently analysed by energy-based methods for free vibration in various degrees-of-freedom. Closed-form analytical expressions exist for the solid–section structural area, neutral axis height, second moment of area in horizontal and vertical bending, polar moment of inertia etc., as shown in Sadowski [18]. For e.g.:

$$\text{Structural area } A(a(x), b(x), p(x), q(x)) \equiv 2ab\frac{\Gamma\left(\frac{1+p}{p}\right)\Gamma\left(\frac{1+q}{q}\right)}{\Gamma\left(\frac{p+pq+q}{pq}\right)},\ \text{Neutral axis } NA(x) \equiv \frac{\frac{1}{4}\frac{1}{q}b}{2\sqrt{\pi}}\frac{\Gamma\left(\frac{2+q}{2q}\right)\Gamma\left(\frac{p+pq+q}{pq}\right)}{\Gamma\left(\frac{2p+pq+q}{pq}\right)},$$

Second moments of area about x -axis and y -axis, and polar moment of area about the centroid (for solid section):

$$I_{bv}(x) \equiv \frac{2ab^3}{q}\frac{\Gamma\left(\frac{3}{q}\right)\Gamma\left(\frac{1+p}{p}\right)}{\Gamma\left(\frac{3p+pq+q}{pq}\right)},\ I_{bh}(x) \equiv \frac{2a^3b}{p}\frac{\Gamma\left(\frac{3}{p}\right)\Gamma\left(\frac{1+q}{q}\right)}{\Gamma\left(\frac{3q+pq+p}{pq}\right)},\ \text{Polar moment of area}$$

$$I_p(x) = I_{bv}(x) + I_{bh}(x) + Ae^2 \tag{2}$$

where A, NA, $I_{bv}(x)$, and $I_{bh}(x)$ give the cross sectional area, the neutral axis, the second moment of area in vertical bending about the deck line, and the second moment of area in horizontal bending about the central line respectively. $I_p(x)$ is the sectional polar moment of inertia, and 'e' is the eccentricity between neutral axis and shear centre. Gamma function $\Gamma(t) = \int_0^\infty x^{t-1}e^{-x}dx$, can be evaluated easily in commercial softwares. This becomes handy for the preliminary estimation of hull girder natural vibration frequencies, at the early stages of design. Storage of section-shapes and hull geometry information is much easier using a semi-rectellipse than by NURBS, because we require only 4 parameters to generate/identify a curve. The reasonably accurate representations of ship geometry help the preliminary designer to conveniently model the arbitrary mass and stiffness distributions over the length of the hull. The import and export of the body-plan of the ship from one software to another requires much less memory and time.

2.2. Geometry of case studies in the project Hull form modelling (actual and mathematical) and properties

The case study of this work is a 7800 TEU containership, as described in Senjanović and Ćatipović [13]. However, since the concept of rectellipses in generating the body plan of a vessel is being attempted for the first time, a few benchmark cases have been studied before the actual case study vessel, with the same dimensions (L = length overall = 334 m, B = moulded breadth = 42.8 m, D = moulded depth = 24.6 m). The shell thickness is considered as 20 mm. The cases considered are:

(a) Fig. 3(a) : Bare hull, semi-ellipsoid (order 2) :

$$\left(\frac{x}{L/2}\right)^2 + \left(\frac{y}{B/2}\right)^2 + \left(\frac{z}{D}\right)^2 = 1,\ \text{Block coefficient } C_b = 0.523. \tag{3a}$$

(b) This gives a semi-ellipsoid, with the same length, breadth and depth of the containership.

(c) Fig. 3(b) : Bare hull, semi-superellipsoid (order 4);

$$\left(\frac{x}{L/2}\right)^4 + \left(\frac{y}{B/2}\right)^4 + \left(\frac{z}{D}\right)^4 = 1,\ \text{Block coefficient } C_b = 0.835 \tag{3b}$$

(d) An increased power in the Lame's curve gives a fuller geometry, as reflected in the block coefficient.

(e) Fig. 3(c) : Uniform (prismatic) bare hull, semi-rectangular channel. Eq.(1) has very high magnitudes of both p and q, say > 20, and thus the rectellipse is almost of a rectangle and hardly an ellipse. The cross-section is uniform throughout the length.

(f) Fig. 3(d) : Uniform (prismatic) bare hull, semi-rectelliptic channel (order 6). Here, $p,\ q\ =\ 3$. This gives a fuller midship section shape than case(a) and case (b). The cross-section is uniform throughout the length.

(g) Fig. 3(e) : Uniform (prismatic) bare hull, semi-circular channel. The cross-section is uniform throughout the length.

(h) Pontoon-type prismatic hull (midship section of 7800 TEU

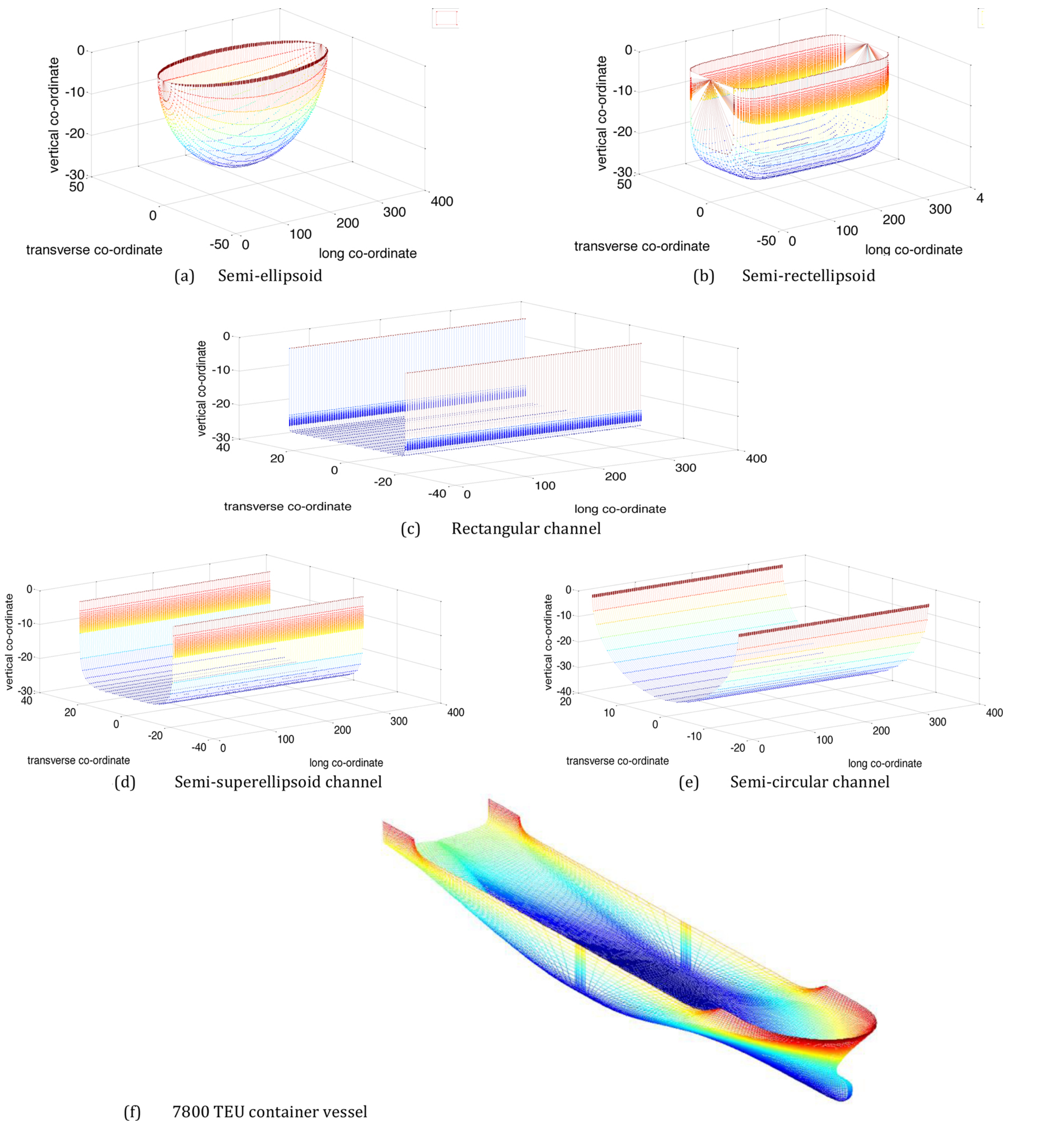

Fig. 3. a) Semi-ellipsoid. b) Semi-rectellipsoid. (c) Rectangular channel.d) Semi-superellipsoid channel. (e) Semi-circular channel. (f) 7800 TEU container vessel.

container vessel extending throughout the length).

(i) Fig. 3(f) : 7800 TEU container vessel (Senjanović and Ćatipović [13]), non-uniform 3D structure, unstiffened bare hull.

Table 1a shows the details of the rectelliptic calculations for the first six benchmark cases. The extreme dimensions and moulded dimensions have both been considered, since the final properties of the thin-walled section is the difference between the properties of extreme and moulded dimensions. Table 1b shows the final sectional properties:

- Sectional material area = Extreme dimensions area – Moulded dimension area;
- Neutral axis from the deck = $\frac{\text{Extreme dimensions area} \times \text{NA}_{\text{extreme}} - \text{Moulded dimension area} \times \text{NA}_{\text{moulded}}}{\text{Sectional material area}}$
- 2nd moment of area about the horizontal axis(m^4) = Extreme dimensions $I_{bv}(x)$ – Moulded dimension $I_{bv}(x)$;
- 2nd moment of area about the vertical axis (m^4) = Extreme dimensions $I_{bh}(x)$ – Moulded dimension $I_{bh}(x)$;

The first 6 cases are symmetric fore-aft. A *semi-ellipsoid* is an order-2 curve which has a finer form, while a *semi-superellipsoid* (order-4) is a fuller form with fore and aft shoulders. Case(a) and Case (b) are for basic studies only. They have no similarity with the containership except for the main dimensions. They are rectellipsoids, instead of being sectionally rectellipses. A semi-rectangular channel (case (c)) is also a rectellipse, of order > 20. A semi-rectelliptic section (case (d)) is a rectellipse of order 4, which will have fuller form as compared to a semi-circular channel of order 2 (case (e)). The pontoon-type prismatic

Table 1a
Geometry of solid section of extreme and moulded dimensions of the benchmark cases.(a–f)

		Case (a) *Semi-ellipsoid*	Case (b) *Semi-rectellipsoid*	Case (c) *Rectangular channel*	Case (d) *Semi-rectelliptic channel*	Case (e) *Semi-circular channel*	Case (f) *Pontoon*
	p	*2*	*4*	*20*	*4*	*2*	*14*
	q	*2*	*4*	*20*	*4*	*2*	*14*
	a (extreme breath/2)	*21.4*	*21.4*	*21.4*	*21.4*	*21.4*	*21.4*
	b (extreme depth)	*24.6*	*24.6*	*24.6*	*24.6*	*24.6*	*24.6*
	a (moulded breath/2)	*21.38*	*21.38*	*21.38*	*21.38*	*21.38*	*21.38*
	b (moulded depth)	*24.58*	*24.58*	*24.58*	*24.58*	*24.58*	*24.58*
Basic Gamma function	$\Gamma(1/q)$	1.773	3.622	19.422	3.622	1.773	13.742
	$\Gamma((p+pq+q)/pq)$	*1.000*	0.886	0.949	0.886	1.000	0.935
	$\Gamma((2+q)/2q)$	0.997	1.227	1.617	1.227	0.997	1.563
	$\Gamma((2p+pq+q)/pq)$	1.330	0.920	0.932	0.920	1.330	0.915
	$\Gamma(3/q)$	0.886	1.227	6.212	1.227	0.886	3.355
	$\Gamma(3/p)$	0.886	1.227	6.212	1.227	0.886	4.355
	$\Gamma((1+p)/p)$	0.886	0.905	0.971	0.905	0.886	0.962
	$\Gamma((1+q)/q)$	0.886	0.905	0.971	0.905	0.886	0.962
	$\Gamma((3p+pq+q)/pq)$	1.994	*1.000*	0.917	1.000	1.994	0.898
	$\Gamma((p+pq+3q)/pq)$	1.994	*1.000*	0.917	1.000	1.994	0.898
	$\Gamma(0.5+1/p)$	0.997	1.227	1.617	1.227	0.997	1.563
Extreme section area	$Area_{extreme} = 2ab\frac{\Gamma\left(\frac{1+p}{p}\right)\Gamma\left(\frac{1+q}{q}\right)}{\Gamma\left(\frac{p+pq+q}{pq}\right)}$	829.46	973.75	1045.82	973.75	829.46	1040.19
	$NA_{extreme} = \frac{\frac{1}{4q}b}{2\sqrt{\pi}}\frac{\Gamma\left(\frac{2+q}{2q}\right)\Gamma\left(\frac{p+pq+q}{pq}\right)}{\Gamma\left(\frac{2p+pq+q}{pq}\right)}$	10.41	11.60	12.25	11.60	10.41	12.24
	2nd moment of area about horizontal neutral axis $\frac{2ab^3}{q}\frac{\Gamma\left(\frac{3}{q}\right)\Gamma\left(\frac{1+p}{p}\right)}{\Gamma\left(\frac{3p+pq+q}{pq}\right)}$	1.255E+05	1.769E+05	2.095E+05	1.769E+05	1.255E+05	1.635E+05
	2nd moment of area about vertical neutral axis $\frac{2a^3b}{p}\frac{\Gamma\left(\frac{3}{p}\right)\Gamma\left(\frac{1+q}{q}\right)}{\Gamma\left(\frac{3q+pq+p}{pq}\right)}$	9.498E+04	1.339E+05	1.586E+05	1.339E+05	9.498E+04	1.606E+05
Moulded section area	$Area_{moulded} = 2ab\frac{\Gamma\left(\frac{1+p}{p}\right)\Gamma\left(\frac{1+q}{q}\right)}{\Gamma\left(\frac{p+pq+q}{pq}\right)}$	828.01	972.05	1044.00	972.05	828.01	1038.37
	$NA_{moulded} = \frac{\frac{1}{4q}b}{2\sqrt{\pi}}\frac{\Gamma\left(\frac{2+q}{2q}\right)\Gamma\left(\frac{p+pq+q}{pq}\right)}{\Gamma\left(\frac{2p+pq+q}{pq}\right)}$	10.40	11.59	12.24	11.59	10.40	12.23
	2nd moment of area about horizontal neutral axis $\frac{2ab^3}{q}\frac{\Gamma\left(\frac{3}{q}\right)\Gamma\left(\frac{1+p}{p}\right)}{\Gamma\left(\frac{3p+pq+q}{pq}\right)}$	1.251E+05	1.764E+05	2.088E+05	1.764E+05	1.251E+05	1.630E+05
	2nd moment of area about vertical neutral axis $\frac{2a^3b}{p}\frac{\Gamma\left(\frac{3}{p}\right)\Gamma\left(\frac{1+q}{q}\right)}{\Gamma\left(\frac{3q+pq+p}{pq}\right)}$	9.464E+04	1.334E+05	1.580E+05	1.334E+05	9.464E+04	1.600E+05

Table 1b
Midship section properties of the benchmark cases.(a–f)

	Case(a)	Case(b)	Case (c)	Case (d)	Case (e)	Case (f)
Sectional material area (m^2)	1.45	1.70	1.83	1.70	1.45	1.82
Neutral Axis (m) from deck (NA)	15.24	16.99	17.95	16.99	15.24	17.93
2nd moment of area about the horizontal axis(m^4)I_{bv}	422.90	596.20	706.00	596.20	422.90	550.96
2nd moment of area about the vertical axis (m^4)I_{bh}	343.07	483.65	572.72	483.65	343.07	580.17

hull (case (f)) has the same midship section as the 7800 TEU container ship. Case (g) is the actual containership hull-form (though minus the internal structures) without fore-aft symmetry. The geometry has been limited to the bare hull for simplicity, since the same aim is to highlight the efficacy of the application of rectellipses, such that this methodology can be applied in practice, particularly in the initial stages of the design spiral. The redistribution of actual hull properties is an important future work. This is a benchmark study of the actual stiffened containership hull, for preliminary estimates of the hull girder frequencies (in various modes), using the Rayleigh-Ritz method, which is supported by geometry definitions using the concept of rectellipses.

In Table 2a, L_{OA} is the overall length, L_{PP} is the length between

Table 2a
Main particulars of the 7800TEU container ship.

L_{OA}	L_{PP}	B	D	L/B	L/D	Draught	Design displacement
334 m	319 m	42.8 m	24.6 m	7.80	13.6	14.5 m	135530 tf (7800 TEU)

Table 2b
Form coefficients of the 7800TEU container ship.

C_B	C_p	C_{wp}	C_m	LCB
0.668	0.675	0.79	0.99	− 1.94 % L_{PP}

Table 3
Midship section properties of the 7800 TEU container ship.

I_P	J	I_w	e	I_{bv}	I_{bh}
334 m^4	14.45 m^4	171400 m^6	25.16 m	676 m^4	1899 m^4

perpendiculars, B is the moulded breath, D is the moulded depth. In Table 2b, C_b is the block coefficient, C_p is the prismatic coefficient, C_M is the midship section area coefficient, C_{wp} is the water plane-area coefficient. In Table 3, 'e' is the distance between the centre of gravity and the shear centre, I_p is the polar moment of area, J is the torsional constant, I_w is the warping constant, I_{bv} is the second moment of cross-sectional area about the horizontal neutral axis (used for vertical vibration), I_{bh} is the second moment of cross-sectional area about the vertical neutral axis (used for horizontal vibration). The axis-system is as follows :

- The $'x'$ -coordinate is along the length. It starts at the midship, is positive towards the forward perpendicular (FP) and negative towards the aft perpendicular (AP) of the mathematical hull. Here, $-\frac{L}{2} < x < \frac{L}{2}$.
- The $'y'$ -coordinate is transverse positive towards the starboard. Here, $-B/2 < y < B/2$.
- The $'z'$ coordinate is vertically upwards. Here, $-D < z < 0$.

A 7800 TEU container vessel from the work by Senjanović and Ćatipović [13] has been studied here. The basic dimensions and owner's requirements of the vessel are tabulated in Table 2**(a)**. The form coefficients of the design vessel are tabulated in Table 2(b). Fig. 4(a) shows the actual NURBS body plan imported from MAXSURF after design. Fig. 4(b) shows the super-elliptic body plan generated using the superellipse methodology explained previously in Section 2. Fig. 4(c) shows hybrid body plan, which is a mixture of Fig. 4(a–b). As far as 60% of stations of the NURBS body plan (Fig. 4(a)) were successfully replicated through semi-superellipses, by choosing appropriate $p(x)$ and $q(x)$ for each station. Fig. 5 shows the longitudinal variation of the super-elliptic powers $p(x)$ and $q(x)$. It can be observed that the parameter $p(x)$ has fractional values closer to the aft sections. This shows that the curve-fitting replicates typical aft sections with the stern overhang. The value of the parameter $q(x)$ has fractional values closer to the fore sections. This shows that the curve-fitting closely replicates the sections with flares in the fore.

The torsion constant including the effects of warping is different from the pure torsion constant (without warping).If warping did not exist, the axial displacement would have been zero. However, a warping function defines the axial deplaning displacement in addition to the twist angle; and is determined from the boundary conditions and compatibility equations. The details are found in Srinath [19]. The torsion constant can be calculated once we know the warping function $\Psi(x, y)$ distribution across the cross section. The torsion constant is

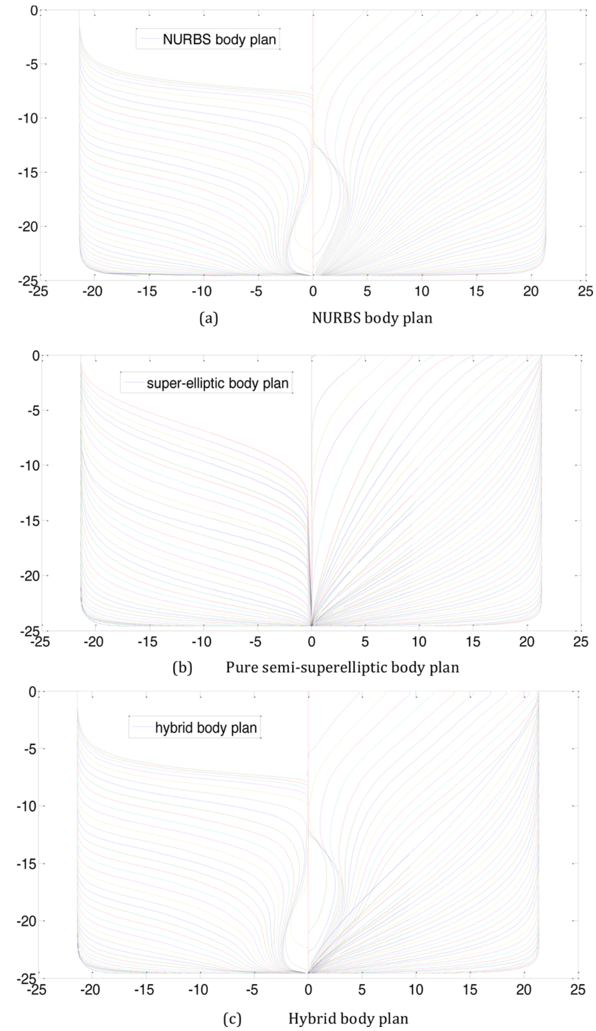

Fig. 4. a)NURBS body plan. (b) Pure semi-superelliptic body plan. (c) Hybrid body plan.

given as $J = \iint_{Area} \left(x^2 + y^2 + x\frac{\partial\Psi(x,y)}{\partial y} - y\frac{\partial\Psi(x,y)}{\partial x}\right)dxdy$. The warping constant is given as $I_w = \iint \Psi^2 dA$. From warping modulus, the warping bimoment is defined as $B_{warp} = -EI_w\frac{\partial^2\Psi}{\partial x^2}$. The rectangular open channel with breadth B, depth D and thickness t has values of shear centre offset from keel as $\frac{D^2B^2t}{4I_{bv}}$, torsion constant and warping modulus values respectively as ;$J = \frac{t^3}{3}(2D + B)$; $I_w = \frac{tD^3B^2}{12}\left(\frac{3D + 2B}{6D + b}\right)$. For the semi-circular open channel with radius r and thickness t, we have shear centre offset from keel as $\left(\frac{4}{\pi} - 1\right)r$; $J = \frac{\pi rt^3}{3}$; $I_w = \frac{2tr^5}{3}\left(\frac{\pi^3}{8} - \frac{12}{\pi}\right)$. If warping was

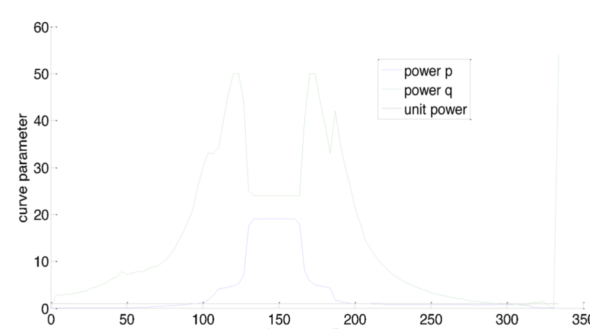

Fig. 5. Longitudinal Distribution of semi-rectellipse powers (order) 'p' and 'q'.

completely restrained, we have $J = \frac{I_p}{\rho}$; where I_p and ρ are polar moment of inertia and density of material (= 7850 kg/m^3, i.e. mild steel) respectively. However, when warping is significant, this value cannot be chosen for torsion constant. The cross-sectional properties (Table 3) thus calculated, have been used in the subsequent vibration analysis.

3. Governing differential equations and boundary conditions for hull girder vibration

The following modes of vibration of the hull have been studied : (i) Vertical (symmetric) vibration : this mode is quite decoupled from the other modes of vibration, (ii) Pure torsional vibration (St. Venant's torsion), (iii) Torsion-warping vibration (Vlasov torsion), (iv) Coupled horizontal-torsional vibration, (v) Coupled horizontal-torsional-warping vibration

3.1. Vertical vibration

Ignoring the effects of shear deformation, the vertical vibratory displacement $w_v(x, t)$ of the non-uniform and uniform beam respectively obeys

$$m(x)\ddot{w}_v(x, t) + E\frac{\partial^2}{\partial x^2}\left(I_{bv}(x)\frac{\partial^2 w_v(x, t)}{\partial x^2}\right) = 0;\ m\ddot{w}_v(x, t) + EI_{bv}\frac{\partial^4 w_v(x, t)}{\partial x^4} = 0 \tag{4a,b}$$

The beam shear force and bending moment are zero at the ends, i.e

$$w_v^{''}(0, t) = w_v^{''}(L, t) = w_v^{'''}(0, t) = w_v^{'''}(L, t) = 0 \tag{4c}$$

There is no axial load on the beam. Pure bending is considered, ignoring shear deformation and rotary inertia. The "thin beam" approximation is assumed here, since the flexural deflections are small. The ship hull is modelled as a *hollow* beam, with intermittent transverse bulkheads (rendering non-uniform mass distribution, *without* affecting the stiffness distribution). Shear stress over each section is maximum at the horizontal neutral axis (NA) which intersects the steel only on the side shell.

3.2. Pure torsional vibration : St Venant's torsion

Ignoring warping, the equation for pure torsion for non-uniform beam is :-

$\rho I_p(x)\frac{\partial^2\Theta(x,t)}{\partial t^2} - G\frac{\partial}{\partial x}\left(J(x)\frac{\partial\Theta(x,t)}{\partial x}\right) = 0$ (5a) where $\Theta(x, t)$ is the twist angle as a function of space and time. All the torque balances are done about the shear centre. Any force acting through the shear centre will not cause any twist in the shape. Though the boundary conditions are same as that of a uniform beam, the modeshapes of non-uniform will not be single cosine/sine function because they are superposition of uniform beam modeshapes. For uniform beams, the equation becomes

$$\rho I_p\frac{\partial^2\theta(x, t)}{\partial t^2} - GJ\frac{\partial^2\theta(x, t)}{\partial x^2} = 0 \tag{5b}$$

The pure twisting torque is zero at the ends, i.e. with the free boundary condition, i.e.

$$GJ\Theta^{'}(0, t) = GJ\Theta^{'}(L, t) = 0 \tag{5c}$$

3.3. Torsional-warping vibration

A circular section will not undergo warping while undergoing torsion. Warping is a sectional deplaning phenomenon [8]. All the moments are balanced about the shear centre of the non-uniform beam. For free vibration, the equation for torsional mode of vibration is given as

$$\rho I_p(x)\frac{\partial^2\Theta(x, t)}{\partial t^2} + E\frac{\partial^2}{\partial x^2}\left(I_w(x)\frac{\partial^2\Theta(x, t)}{\partial x^2}\right) - G\frac{\partial}{\partial x}\left(J(x)\frac{\partial\Theta(x, t)}{\partial x}\right) = 0 \tag{6a}$$

For uniform beams, the equation simplifies as

$$\rho I_p\frac{\partial^2\theta(x, t)}{\partial t^2} + EI_w\frac{\partial^4\theta(x, t)}{\partial x^4} - GJ\frac{\partial^2\theta(x, t)}{\partial x^2} = 0 \tag{6b}$$

The beam is subject to the boundary conditions of bimoment and total twisting moment equal to zero at the ends. With free edge condition (the normal stress due to warping at the free edge is zero; and also the total twisting moment is zero at the ends):

$$EI_w\Theta^{''}(0, t) = EI_w\Theta^{''}(L, t) = 0;\ EI_w\Theta^{'''}(0, t) - GJ\Theta^{'}(0, t) = EI_w\Theta^{'''}(L, t) - GJ\Theta^{'}(L, t) = 0 \tag{6c}$$

This is in accordance with Bishop et al [5], and thus an improvement over Li et al [1], Senjanović and Ćatipović [13], who generate the modeshape by withholding warping, thereby simplifying Eq. 6(c) to $\Theta^{'''}(0, t) = \Theta^{'}(0, t) = \Theta^{'''}(L, t) = \Theta^{'}(L, t) = 0$.

3.4. Horizontal vibration

The horizontal vibration has the same governing differential equation and boundary conditions as the vertical vibration, but the geometric properties get changed. Ignoring the effects of shear deformation, the horizontal vibratory displacement $w_b(x, t)$ of the non-uniform and uniform beam respectively obeys

$$m(x)\ddot{w}_b(x, t) + E\frac{\partial^2}{\partial x^2}\left(I_{bh}(x)\frac{\partial^2 w_b(x, t)}{\partial x^2}\right) = 0;\ m\ddot{w}_b(x, t) + EI_{bh}\frac{\partial^4 w_b(x, t)}{\partial x^4} = 0\,(7(a, b)) \tag{7a,b}$$

At the two free ends, the shear force and bending moment are zero, i.e.

$$EI_{bh}(0)w_b^{''}(0, t) = EI_{bh}(L)w_b^{''}(L, t) = EI_{bh}(0)w_b^{'''}(0, t) = EI_{bh}(L)w_b^{'''}(L, t) = 0 \tag{7c}$$

3.5. Pure torsion-horizontal coupled vibration

The pair of coupled horizontal-torsional vibration governing differential equations are :

$$m(x)\ddot{w}_b(x, t) + E\frac{\partial^2}{\partial x^2}\left\{I_{bh}(x)\frac{\partial^2 w_b(x, t)}{\partial x^2}\right\} + m(x)c(x)\frac{\partial^2\Theta(x, t)}{\partial t^2} = 0;\ \rho I_p(x)\frac{\partial^2\Theta(x, t)}{\partial t^2} - G\frac{\partial}{\partial x}\left\{J(x)\frac{\partial\Theta(x, t)}{\partial x}\right\} + m(x)c(x)\frac{\partial^2 w_b(x, t)}{\partial t^2} = 0 \tag{8a,b}$$

For the uniform beam,

$$m\ddot{w}_b(x, t) + EI_{bh}\frac{\partial^4 w_b(x, t)}{\partial x^4} + mc\frac{\partial^2\theta(x, t)}{\partial t^2} = 0;\ \rho I_p\frac{\partial^2\theta(x, t)}{\partial t^2} - GJ\frac{\partial^2\theta(x, t)}{\partial x^2} + mc\frac{\partial^2 w_b(x, t)}{\partial t^2} = 0 \tag{8c,d}$$

At the free ends, the horizontal shear force, the bending moment, and the twisting torque are zero. The boundary conditions are:

$$EI_{bh}(0)w_b^{''}(0, t) = EI_{bh}(L)w_b^{''}(L, t) = 0;\ EI_{bh}(0)w_b^{'''}(0, t) = EI_{bh}(L)w_b^{'''}(L, t) = 0;\ GJ\Theta^{'}(0, t) = GJ\Theta^{'}(L, t) = 0 \tag{8e}$$

3.6. Torsion-warping-horizontal coupled vibration

The eccentricity of the shear centre from the neutral axis cause significant dynamic coupling between torsional and horizontal mode of vibration. The force and moment balance yields the system of equations for coupled mode of vibration :

$$m(x)\ddot{w}_b(x,t) + E\frac{\partial^2}{\partial x^2}\left\{I_{bh}(x)\frac{\partial^2 w_b(x,t)}{\partial x^2}\right\} + m(x)c(x)\frac{\partial^2\Theta(x,t)}{\partial t^2} = 0 \quad (9a)$$

$$\rho I_p(x)\frac{\partial^2\Theta(x,t)}{\partial t^2} + E\frac{\partial^2}{\partial x^2}\left\{I_w(x)\frac{\partial^2\Theta(x,t)}{\partial x^2}\right\} - G\frac{\partial}{\partial x}\left\{J(x)\frac{\partial\Theta(x,t)}{\partial x}\right\} + m(x)c(x)\frac{\partial^2 w_b(x,t)}{\partial t^2} = 0 \quad (9a,b)$$

For the uniform beam, the force and moment balance equations are

$$m\ddot{w}_b(x,t) + EI_{bh}\frac{\partial^4 w_b(x,t)}{\partial x^4} + mc\frac{\partial^2\theta(x,t)}{\partial t^2} = 0;\ \rho I_p\frac{\partial^2\theta(x,t)}{\partial t^2} + EI_w\frac{\partial^4\theta(x,t)}{\partial x^4} - GJ\frac{\partial^2\theta(x,t)}{\partial x^2} + mc\frac{\partial^2 w_b(x,t)}{\partial t^2} = 0 \quad (9c,d)$$

$I_p(x)$ is calculated about the shear centre and not the centre of gravity. If the shear centre S is very close to the centre of gravity C, i.e., $c(x) \to 0$, leading to the decoupling of the above system of equations. This is true for closed-section tankers, in which C and S to almost coincide. However, for open section containerships, the distance between C and S is of the order of depth D, leading to a strong coupling between the two modes of vibration. The boundary conditions are (i) the warping bimoment is zero (it is free to warp), (ii) the total twisting moment is zero (it is free to turn), and (iii) the horizontal shear force and bending moment are zero (not constrained against translation and rotation); at the two ends. Thus, the boundary conditions are a combination of Eq.6(c) and Eq.7(c). The admissible functions or modeshapes should satisfy all 8 boundary conditions (shear force, bending moment is zero at the ends; warping bimoment and total twisting torque is zero at the ends).

4. Solution methodology

Three methodologies have been used here : frequency search method, Rayleigh-Ritz method, and FEM. “Frequency search” is the already existing method for solving coupled vibration for uniform beams. However, the method does not work for a non-uniform beam. FEA can be used for coupled non-uniform beam; however, the process is computationally expensive. Rayleigh-Ritz is the method being proposed through this work. The method works for solving coupled non-uniform vibration and requires much less computational time than FEA and gives reasonably accurate results. The frequency search method will be used for the following cases: torsion-warping, torsion-horizontal coupled and torsion-warping-horizontal coupled vibration of uniform beam modes. The details are found in Bishop et al [5].

4.1. Rayleigh-Ritz method

The Rayleigh-Ritz method to analyse vertical plane vibration of non-uniform beam is shown below. The methodology can be used for pure torsional, torsion-warping and coupled torsion-warping-horizontal vibration of non-uniform beams.

4.1.1. Vertical Vibration/Horizontal vibration

Assuming small-amplitude displacements, where linear superposition holds, the total flexural displacement $w_v(x,t)$ in Eq. (4(a)) can be assumed to be a superposition of the modal displacements

$$w_v(x,t) = \sum_{j=1}^{\infty}\Phi_j(x)q_j(t) \quad (10a)$$

where $\Phi_j(x)$ is the jth *non-uniform* beam mode and $q_j(t)$ is the jth principal coordinate, harmonic in time. $\Phi_j(x)$ is a weighted sum of the admissible functions (uniform beam modeshapes), i.e.

$$\Phi_j(x) = \sum_{k=1}^{\infty}a_{jk}\varphi_k(x) \quad (10b)$$

where $\varphi_k(x)$ is the kth ***uniform*** vertical vibration beam modeshape, satisfying $\varphi_k^{''}(0) = 0$, $\varphi_k^{''}(L) = 0$, $\varphi_k^{'''}(0) = 0$, $\varphi_k^{'''}(L) = 0$; and a_{jk} is the unknown weight of the contribution of the $\varphi_{kv}(x)$ to the jth non-uniform beam modeshape.

Admissible function

$$\varphi_j(x) = cos(\gamma_j x) + \cosh(\gamma_j x) + \upsilon_j[sin(\gamma_j x) + sinh(\gamma_j x)];\ \upsilon_j = \frac{\sin\gamma_j L + \sinh\gamma_j L}{\cos\gamma_j L - \cosh\gamma_j L} \quad (10c)$$

Here, $\varphi_j(x)$ acts as the jth admissible function to the series sum (Eq. 10(b)), and satisfies the boundary conditions.

Now, let $w_v(x,t) = Z(x)cos\omega t$, where $Z(x)$ is an assumed shape function and ω is the circular frequency.

Total potential and kinetic energy:

$$U = \left\{\frac{1}{2}\int_{x=0}^{x=l}EI(x)\left[\frac{d^2Z(x)}{dx^2}\right]^2dx\right\}cos^2\omega t\ ;\ T = \omega^2\left\{\frac{1}{2}\int_{x=0}^{x=l}m(x)[Z(x)]^2dx\right\}sin^2\omega t \quad (10d)$$

In a conservative system, $U_{max} = T_{max}$. Thus, the circular frequency is expressed as

$$\omega^2 = \frac{\frac{1}{2}\int_{x=0}^{x=l}EI(x)\left[\frac{d^2Z(x)}{dx^2}\right]^2dx}{\frac{1}{2}\int_{x=0}^{x=l}m(x)[Z(x)]^2dx} \quad (10e)$$

The exact solution for the frequency would be that of the modeshape which minimizes the frequency. In order to reach the minimum frequency, we assume $Z_V(x) = \sum_{k=1}^{\infty}a_k\varphi_k(x)$. The unknown coefficients a_{jk} are calculated by minimizing the frequency with respect to each coefficient. Applying the Ritz method

$$\frac{\partial}{\partial a_k}\left\{\frac{\frac{1}{2}\int_{x=0}^{x=l}EI(x)\left[\frac{d^2Z_V(x)}{dx^2}\right]^2dx}{\frac{1}{2}\int_{x=0}^{x=l}m(x)[Z_V(x)]^2dx}\right\} = 0 \quad (10f)$$

The equation reduces to

$$\frac{\partial}{\partial a_k}\left\{\frac{1}{2}\int_{x=0}^{x=l}EI(x)\left[\frac{d^2Z_V(x)}{dx^2}\right]^2dx - \omega^2\frac{1}{2}\int_{x=0}^{x=l}m(x)[Z_V(x)]^2dx\right\} = 0 \quad (10g)$$

Using generalized mass and generalized stiffness $\beta_{jk} = \int_0^L m(x)\varphi_j(x)\varphi_k(x)dx$; $\alpha_{jk} = \int_0^L EI(x)\varphi_j^{''}(x)\varphi_k^{''}(x)dx$, respectively, the above set of equations reduces to : $\sum_{k=1}^{N}a_j(\alpha_{jk} - \lambda\beta_{jk}) = 0$ which is solved for ‘j’ number of equations. Here, $\lambda = \omega^2$. The determinant of the square matrix, when equated to zero, gives the frequency equation. This gives an Nth order equation in λ, and solving it generates ‘N’ number of roots : $\lambda_1, \lambda_2, \lambda_3, \ldots\ldots, \lambda_N$. For $1 \le k \le N$, we input λ_k into the system of equations, in order to re-generate the N × N matrix. Each row corresponds to one Eigen-vector, i.e. a_1: a_2: a_3: ……:a_k: …..:a_N. The details may be found in Timoshenko [20]. In the application of the Rayleigh-Ritz method to other modes of vibration, the basic methodology of remains unchanged. First, the uniform modeshapes are generated andthe non-uniform modeshape is expressed as their weighted sum. The maximum potential energy and kinetic energy are expressed in terms of the unknown non-uniform modeshape, and the natural frequencies are minimized w.r.t. the unknown coefficients. This generates the non-uniform frequencies, and leads to the non-uniform modeshapes.

4.1.2. Pure torsional vibration (St. Venant’s torsion)

Assuming small-amplitude displacements, where linear superposition holds, the total angular displacement $\mathbf{\Theta}(x,t)$ in Eq. 5(a) can be assumed to be a superposition of the modal displacements : $\mathbf{\Theta}(x,t) = \sum_{j=1}^{\infty}\Theta_j(x)q_j(t)$, where $\Theta_j(x)$ is the jth *non-uniform* torsional beam mode and $q_j(t)$ is the j[th] principal coordinate, harmonic in time. $\Theta_j(x)$ is a weighted sum of the admissible functions (uniform torsional beam modeshapes), i.e., $\Theta_j(x) = \sum_{k=1}^{\infty} a_{jk}\theta_k(x)$ where $\theta_k(x)$ is the k[th] *uniform* torsional vibration beam modeshape, and a_{jk} is the unknown weight of the contribution of the $\theta_k(x)$ to the j[th] non-uniform torsional beam modeshape. The admissible function is $\theta(x) = \cos(\gamma_j x)$, satisfying the boundary conditions $GJ(0)\theta'(0, t) = GJ(L)\theta'(L, t) = 0$; where $\gamma_j = (2j+1)\frac{\pi}{2}$.

The energies are : $T = \frac{1}{2}\left[\int_{x=0}^{l} \{\rho I_p(x)(\Theta(x))^2\}dx\right] \sin^2\omega t$; $U = \frac{1}{2}\left[\int_{x=0}^{l}\left\{GJ\left(\frac{\partial\Theta(x)}{\partial x}\right)^2\right\}dx\right]\cos^2\omega t$

4.1.3. Torsion-warping vibration (Vlasov torsion)

When warping is not considered, the pure torsion modeshapes of a uniform free-free beam is $\theta_j(x) = \cos(\gamma_j x)$. The other waveforms become non-zero when warping is included (**Eq.6(a)**). Thus, the admissible function is:

$$\theta_j(x) = H_1 \cosh(\gamma_j x) + H_2 \sinh(\gamma_j x) + H_3 \cos(\delta_j x) + H_4 \sin(\delta_j x);\ \text{where}\ \gamma_j, \delta_j = \frac{GJ}{2EI_w} \mp \sqrt{\left(\left(\frac{GJ}{2EI_w}\right)^2 + \frac{\omega^2\rho I_p}{EI_w}\right)}$$

are the wave numbers. From the boundary conditions in Eq.(6(c)),

$$H_3 = 1;\ H_1 = \frac{\delta^2}{\gamma^2}H_3;\ H_2 = \frac{-H_1\gamma^2\cosh(\gamma L) + H_3\delta^2\cos(\delta L)}{\gamma^2\sinh(\gamma L) - \delta^2\sin(\delta L)\left(\frac{\gamma^3 - \frac{GJ}{EI_w}\gamma}{\delta^3 + \frac{GJ}{EI_w}\delta}\right)};\ H_4 = H_2\left(\frac{\gamma^3 - \frac{GJ}{EI_w}\gamma}{\delta^3 + \frac{GJ}{EI_w}\delta}\right)$$

The energies are:

$$T = \frac{1}{2}\left[\int_{x=0}^{l}\{\rho I_p(x)\Theta(x)^2\}dx\right]\sin^2\omega t;\ U = \frac{1}{2}\left[\int_{x=0}^{l}\left\{GJ\left(\frac{\partial\Theta(x)}{\partial x}\right)^2 + EI_w\left(\frac{\partial^2\Theta(x)}{\partial x^2}\right)^2\right\}dx\right]\cos^2\omega t$$

4.1.4. Coupled horizontal-torsional vibration

The admissible function for horizontal vibration in Eq. 8(a) is : $\varphi_j(x) = \cos(\gamma_j x) + \cosh(\gamma_j x) + \upsilon_j[\sin(\gamma_j x) + \sinh(\gamma_j x)]$;

$\upsilon_j = \frac{\sin\gamma_j L + \sinh\gamma_j L}{\cos\gamma_j L - \cosh\gamma_j L}$; $\cos(\gamma_j L)\cosh(\gamma_j L) = 1$. The admissible function for torsional vibration in Eq.8(b) is : $\theta_j(x) = \cos(\gamma_j x)$, satisfying the boundary conditions $\theta'(0, t) = \theta'(L, t) = 0$; where $\gamma_j = (2j+1)\frac{\pi}{2}$.

The kinetic and potential energies respectively are:

$$T = \frac{1}{2}\left[\int_{x=0}^{l}\{\rho I_p(x)(\Theta(x))^2 + m(x)(Z_H(x))^2 + 2mc\Theta(x)Z_H(x)\}dx\right]\sin^2\omega t;$$

$$U = \frac{1}{2}\left[\int_{x=0}^{l}\left\{GJ\left(\frac{\partial\Theta(x)}{\partial x}\right)^2 + EI_{bh}\left(\frac{\partial^2 Z_H(x)}{\partial x^2}\right)^2\right\}dx\right]\cos^2\omega t$$

4.1.5. Coupled horizontal-torsional warping vibration

The admissible functions are the same as in Sec 4.2.1 and 4.2.3. The kinetic and potential energies respectively are :

$$T = \frac{1}{2}\left[\int_{x=0}^{l}\{\rho I_p(x)(\Theta(x))^2 + m(x)(Z_H(x))^2 + 2mc\Theta(x)Z_H(x)\}dx\right]\sin^2\omega t$$

$$U = \frac{1}{2}\left[\int_{x=0}^{l}\left\{GJ\left(\frac{\partial\Theta(x)}{\partial x}\right)^2 + EI_w\left(\frac{\partial^2\Theta(x)}{\partial x^2}\right)^2 + EI_{bh}\left(\frac{\partial^2 Z_H(x)}{\partial x^2}\right)^2\right\}dx\right]\cos^2\omega t$$

4.2. Finite element method

Every beam element has four boundary conditions at each node : (a) bending deflection, (b) bending slope, (c) twisting deflection and (d) twisting slope. A 2-noded finite element is chosen, with eight degrees of freedom (DOF). The bending deflection is given by the polynomial : $w_b = a_1 + a_2 x + a_3 x^2 + a_4 x^3$, while the twisting deflection is given by : $\Theta = b_1 + b_2 x + b_3 x^2 + b_4 x^3$. The bending and twisting slopes are given by $\frac{\partial w_b}{\partial x}$ and $\frac{\partial \Theta}{\partial x}$ respectively. The energies that contribute towards the consistent mass matrix are:

Torsion inertia energy $T_1 = \frac{1}{2}\left[\int_{x=0}^{l}\rho I_p(x)(\Theta(x))^2 dx\right]\sin^2\omega t$. Bending inertia energy $T_2 = \frac{1}{2}\left[\int_{x=0}^{l} m(x)(w_b(x))^2 dx\right]\sin^2\omega t$.

Coupling inertia energy $T_3 = \frac{1}{2}\left[\int_{x=0}^{l}\{2mc\Theta(x)w_b(x)\}dx\right]\sin^2\omega t$. The energies contributing towards the stiffness matrix are :

Twisting strain energy $U_1 = \frac{1}{2}\left[\int_{x=0}^{l} GJ\left(\frac{\partial\Theta(x)}{\partial x}\right)^2 dx\right]\cos^2\omega t$. Bending strain energy $U_3 = \frac{1}{2}\left[\int_{x=0}^{l} EI_{bh}\left(\frac{\partial^2 Z_H(x)}{\partial x^2}\right)^2 dx\right]\cos^2\omega t$.

Warping stiffness strain energy $U_2 = \frac{1}{2}\left[\int_{x=0}^{l} EI_w\left(\frac{\partial^2\Theta(x)}{\partial x^2}\right)^2 dx\right]\cos^2\omega t$. The combination of the energies are as follows :

Pure torsional vibration (St. Venant): $T = T_1$; $U = U_1$. Torsion-warping vibration (Vlasov) : $T = T_1$; $U = U_2 - U_1$

Coupled horizontal-torsional vibration : $T = T_1 + T_2 + T_3$; $U = U_1 + U_3$

Coupled horizontal-torsional warping vibration : $T = T_1 + T_2 + T_3$; $U = U_2 - U_1 + U_3$

Table 4
Vertical vibration frequencies (rad/s) by Rayleigh-Ritz and FEA for all cases of uniform beam.

Semi- circular channel (Case(e))		Rectelliptic channel of order 4 (Case (d))		Pontoon (Case(f))	
Rayleigh-Ritz	FEA	Rayleigh-Ritz	FEA	Rayleigh-Ritz	FEA
15.218	15.218	17.769	17.769	10.640	10.641
41.950	41.950	48.981	48.982	29.331	29.331
83.238	82.240	96.023	96.025	57.500	57.502
139.44	135.95	158.731	158.742	95.051	95.058
203.077	203.11	237.117	237.153	141.990	142.012

Table 5
Vertical vibration frequencies (rad/s) by Rayleigh-Ritz and FEA for the non-uniform beam.

Semi- rectellipsoid (Case(b))					7800 TEU Container ship (Case(g))				
Uniform (Euler-Bernoulli)	Rayleigh-Ritz	FEA	% error (uniform)	% error (Ritz)	Uniform (Euler-Bernoulli)	Rayleigh-Ritz	FEA	%error (uniform)	%error (Ritz)
17.769	18.766	19.203	7.47	2.28	10.641	11.802	11.862	10.3	0.5
48.982	50.941	52.296	6.34	2.59	29.331	29.947	30.216	2.93	0.89
96.025	99.035	101.46	5.36	2.39	57.502	56.405	56.002	2.68	0.72
158.74	162.015	166.34	4.57	2.6	95.058	89.775	89.231	6.53	0.61
237.15	240.615	246.92	3.96	2.55	142.01	131.442	130.391	8.92	0.8

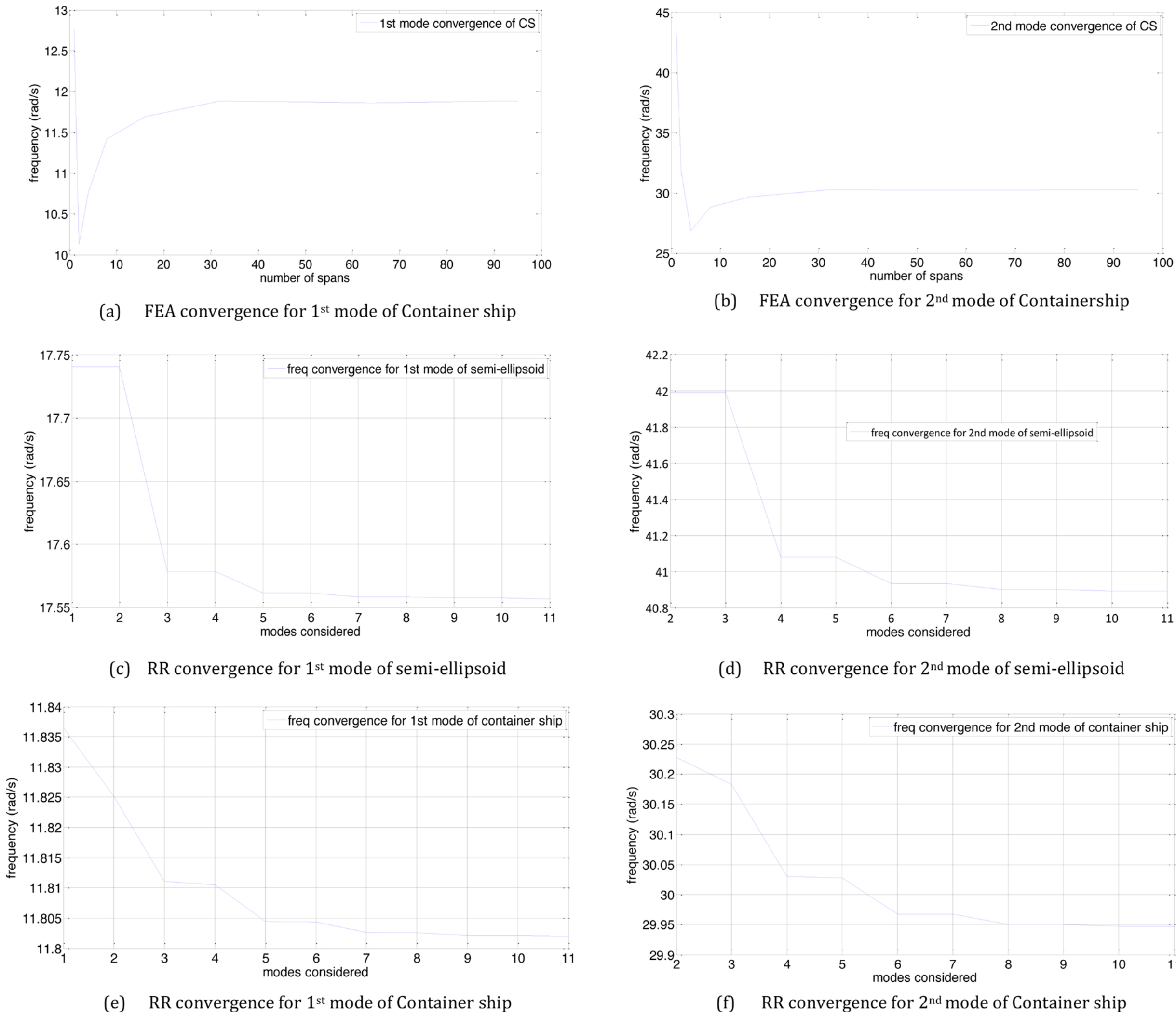

(a) FEA convergence for 1st mode of Container ship

(b) FEA convergence for 2nd mode of Containership

(c) RR convergence for 1st mode of semi-ellipsoid

(d) RR convergence for 2nd mode of semi-ellipsoid

(e) RR convergence for 1st mode of Container ship

(f) RR convergence for 2nd mode of Container ship

Fig. 6. a) FEA convergence for 1st mode of Container ship. (b) FEA convergence for 2nd mode of Containership (c) RR convergence for 1st mode of semi-ellipsoid.(d) RR convergence for 2nd mode of semi-ellipsoid.(e)RR convergence for 1st mode of Container ship. (f) RR convergence for 2nd mode of Container ship.

The total energy matrices form an Eigen value problem which leads to the natural frequencies.

5. Results

5.1. Vertical vibration

Table 4 shows the comparative vertical vibration frequencies of the simplest benchmark cases, by the Rayleigh-Ritz method and FEA, for the three *uniform* beams, i.e. semi-circular channel, rectelliptic channel of order 4, and pontoon. Since the beams are uniform, the Rayleigh-Ritz method generates a diagonal weight matrix. Table 5 shows the comparative vertical vibration frequencies by the Rayleigh-Ritz method and FEA, for the non-uniform hulls, i.e. the semi-rectellipsoid and the 7800 TEU containership. The close correlation between the two methods shows the efficacy of our approach. The Rayleigh-Ritz approach of non-uniform hull vibration analysis provides a significant improvement over the uniform beam analysis, especially in the identification of the fundamental frequency. The details are found in Datta and Thekinen [16].

Fig. 6(a,b) shows the FEA convergence of 1st and 2nd modes of vertical vibration the containership for increasing number of elements/spans. Convergence is seen to arrive at 40 elements or so. Fig. 6(c,d) shows the Rayleigh-Ritz frequency convergence for the fundamental mode and the first overtone of the semi-ellipsoid as a function of

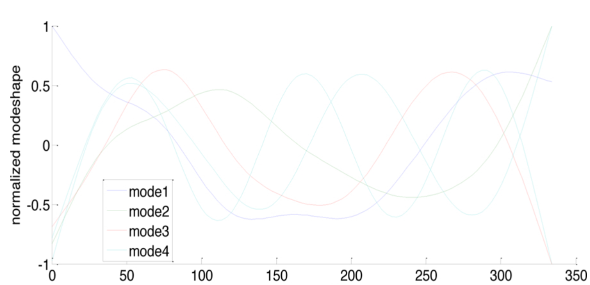

Fig. 7. RR first five(5) vertical vibration modes of Container ship.

Table 6a
1st five pure torsion frequencies (rad/s) of uniform beam.

RectangularChannel (Case(c))	Circular Channel (Case(e))	Pontoon (Case(f))	FEA	% error
29.877	29.877	29.877	29.877	1.2×10^{-7}
59.753	59.753	59.753	59.753	7.4×10^{-6}
89.63	89.63	89.63	89.63	7.9×10^{-5}
119.506	119.506	119.506	119.507	4.1×10^{-4}
149.383	149.383	149.383	149.385	1.42×10^{-3}

Table 6b
1st five pure torsion frequencies (rad/s) of non-uniform beam.

Pontoon (Case(f))	Container ship (Ritz) (Case(g))	Container ship (FEA) (Case(g))	% error (uniform)	%error (Ritz)
29.877	36.545	36.635	18.449	0.246
59.753	64.386	67.93	11.598	4.743
89.63	96.793	97.174	7.764	0.393
119.506	123.640	126.573	5.583	2.318
149.383	155.391	156.029	4.260	0.409

number of modes considered. The first frequency converges for 7 modes, while the second one for 8 modes. This is a marked computational improvement over the FEA. For a 3D body with fore and aft symmetry, only odd admissible functions contribute towards odd non-uniform frequency and modeshape; and vice-versa with even modeshapes. This can be observed that the frequency convergence curve for fundamental mode is undisturbed from modes 1 to 2, then from modes 3 to 4, and so on. Further for the 2nd mode, the same happens from mode 2 to 3, then from mode 4 to 5, etc.

Fig. 6(e,f) shows the Rayleigh-Ritz frequency convergence for the fundamental mode and the first overtone of the containership as a function of number of modes. The first frequency is seen to converge for 9 modes, while the second one for 10 modes. For the container ship, there is no fore and aft symmetry. Hence all the modes contribute towards both odd and even non-uniform modeshapes. Odd uniform modes significantly contribute towards odd non-uniform modeshape, and even uniform modes significantly contribute towards the even non-uniform modeshapes.

Fig. 7 shows the first 5 vertical non-uniform modeshapes of the Containership, obtained from the Rayleigh-Ritz method. They lack fore-aft symmetry/anti-symmetry. The number of nodes helps us recognize the sequence of the modes. The distortions in the shape are due to the presence of k^{th} uniform mode(s) in the j^{th} non-uniform mode. The fundamental modeshape sees the maximum distortion. The higher-order non-uniform modes show less distortion. Thus, the first non-uniform frequency should show the maximum deviation from the first uniform frequency.

5.2. Torsional and torsion-warping vibration

The pure torsion frequencies for first five modes of the uniform beams are tabulated in Table 6a. The frequencies are unchanged on varying the cross sectional properties in the case of St. Venant's torsion. This is because the frequency depends only on the length of the beam and is independent of torsion constant and polar moment of inertia. The pure torsion frequencies for first five modes of the non-uniform 7800 TEU containership are tabulated in Table 6b . Using the information from Tables 2a,b-3, the two approaches are seen to produce close results, with the R-R method efficient over FEA.

The first five torsion-warping (Vlasov torsion) frequencies for various uniform beams are calculated using frequency search method, Rayleigh-Ritz method, and FEA. Comparisons are made in Table 7a. It is seen that all three methods fetch identical results for uniform beams.

Table 7b
1st five torsion-warping frequencies (rad/s).

7800 TEU Container ship (Case(g))				
Freq search	*Ritz*	*FEA*	*% error (search)*	*%error (Ritz)*
10^{-8}	0	0	0	0
2.449	3.312	3.295	25.67	0.5
9.808	13.78	13.62	27.99	1.15
24.43	31.75	31.32	21.99	1.39
46.65	56.74	55.92	16.57	1.47

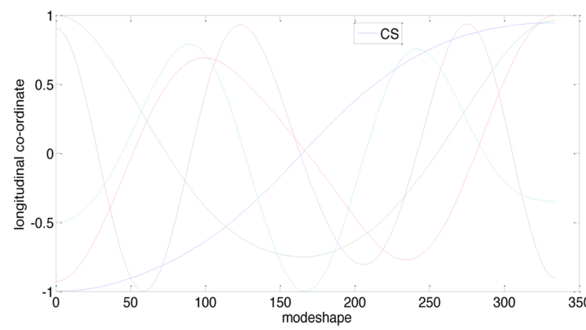

Fig. 8. First five (5) torsion modeshapes of Container ship.

Table 8
Beam characteristics.

Parameter	Dimension
Length	1.28 m
Breadth	0.1 m
Depth	0.058 m
thickness	0.00125 m

Table 9
First four St.Venant's and Vlasov torsion frequencies of rectangular channel (Case(c)).

Mode	Present (no warping)	Bishop [5]	% error	Present (with warping)	Bishop [5]	% error (St. Venant)	% error (Vlasov)
Mode1	124.65	122.78	1.515	138.06	135.96	9.31	1.54
Mode2	190.47	189.48	0.005	939.76	939.76	397.07	0.00
Mode3	287.27	285.7	0.55	2547.27	2547.4	789.36	0.005
Mode4	381.19	–	–	3872.44	–	–	–

Comparisons of the first five torsion-warping (Vlasov torsion) frequencies for the non-uniform 7800 TEU container ship are tabulated in Table 7b. From the % error from FEA results, it is clear that Rayleigh-Ritz method offer significant advantage over frequency search method when the beam is non-uniform. Another interesting point from Table (7a,b) is that allowing for warping reduces the frequencies by a significant magnitude. Pure torsion is equivalent to restraining warping by

Table 7a
1st five torsion-warping frequencies (rad/s) of uniform beam.

Rectangular Channel (Case(c))			Circular Channel (Case(e))			Pontoon (Case(f))		
Freq search	*Ritz*	*FEA*	*Freq search*	*Ritz*	*FEA*	*Freq search*	*Ritz*	*FEA*
0.012	0.012	0.012	0.0009	0.0009	0.0009	10^{-8}	10^{-8}	10^{-8}
5.883	5.883	5.883	0.171	0.171	0.171	2.449	2.449	2.449
16.22	16.22	16.22	0.472	0.472	0.472	9.808	9.808	9.808
31.79	31.79	31.79	0.926	0.926	0.926	24.43	24.43	24.43
52.55	52.55	52.55	1.53	1.53	1.53	46.65	46.65	46.65

Table 10
Comparison for uncoupled torsion-warping frequencies with horizontal-torsion-warping coupled ones.

Rectangular Channel (Case(c))			Circular Channel (Case (e))			Pontoon (Case(f))		
Un-couple	couple	% error	Un-couple	couple	% error	Un-couple	couple	% error
5.883	5.718	2.88	0.171	0.17	0.75	2.449	5.867	58.27
16.22	15.756	2.92	0.472	0.469	0.73	9.808	14.694	33.25
31.79	24.2	31.37	0.926	0.919	0.72	24.43	28.075	12.99
52.55	30.89	70.14	1.53	1.519	0.73	46.65	29.463	58.34

Table 11
Comparison of frequencies for 2 BCs adopted for the 7800 TEU containership (Case(g)).

Free warping			Restrained warping		% difference
Frequency search	FEA	% diff	Frequency search	Senjanovic [13]	Free vs. restrained
0.4671	0.4671	0	0.893	0.893	91.18
2.0164	2.0277	0.56	3.250	3.250	60.28
5.1004	5.1345	0.67	7.172	7.172	39.68
9.784	9.852	2.06	12.662	12.662	28.52
16.044	16.159	0.72	19.720	19.720	22.04
23.877	24.052	0.73	28.346	28.346	17.85
33.281	33.530	0.75	38.541	38.541	14.95
44.255	44.597	0.77	50.304	50.304	11.89

Table 12
Comparison of frequencies for various analysis methodologies (Pontoon hull (Case(f))).

Analysis type	Mode1		Mode2		Mode3	
	freq	% error	freq	% error	freq	% error
Pure torsion	29.877	409	59.753	309.65	89.63	219.25
Torsion-horizontal	1.28	78	17.51	19.16	32.29	15.01
Torsion-warping	2.449	58.26	9.81	33.23	24.43	12.98
Torsion-warping-horizontal	5.867	–	14.69	–	28.08	–

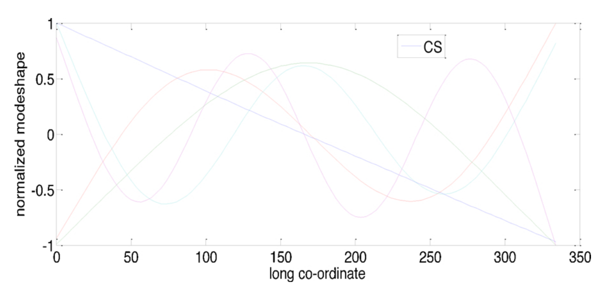

Fig. 9. 1st five(5)non-uniform modes of torsion-warping vibration of the Containership.

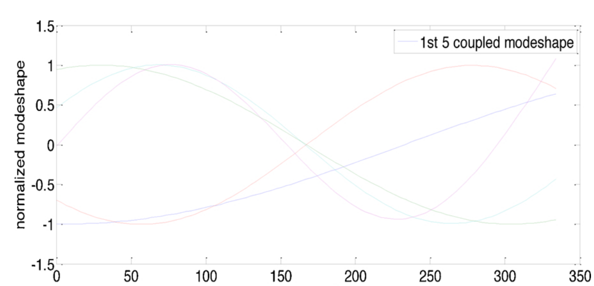

Fig. 10. 1stfive(5) uniform beam modeshapes of torsion-warping-horizontal coupled vibration.

assuming infinite warping stiffness. Fig.8 shows the first five torsion modeshapes.

5.3. Coupled torsion-horizontal vibration

As a case study, the torsion-horizontal frequencies for a rectangular channel (dimensions in Table 8) are obtained and compared with Bishop (1988). For the 1st four frequencies of pure torsion and Vlasov torsion are compared (Table 9). This again shows the efficacy of the present approach. For open sections, ignoring the effect of coupling of horizontal and torsional modes may result in substantially different frequencies. This is illustrated in Table 10. The 1st four uncoupled torsion-warping frequencies are compared with horizontal-torsion-warping coupled frequencies for various prismatic geometries. Only a circular channel has a negligible difference, because the centre of gravity and shear centre coincide, leading to decoupling of the two modes.

There can be three categories of classical boundary conditions as elaborated. For torsion-warping, [13] chose free twisting and restrained warping for ship-like girders; and obtained the frequencies tabulated above for a pontoon with the same midship-section properties, but with length 300 m. The procedure was followed using free warping and free twisting boundary conditions, using frequency search and FEA. The results are compared in Table 11.

For various analysis methodologies in Section 4.2.2-4.2.5, the deviation of each ‘restricted’ frequency (pure torsion, torsion-horizontal, and torsion-warping) from the most generic torsion-warping-horizontal coupled frequency is shown for the 1st three frequencies of a pontoon type hull (Table 12). They satisfy all the eight boundary conditions. Fig. 9 shows the first five modeshapes of torsion-warping vibration of the containership. Fig. 10 shows the first five uniform beam modeshapes of the coupled horizontal-torsion-warping vibration of the containership, which are used in the Rayleigh-Ritz method as admissible functions, as shown in Sec. 4.2.5.

6. Summary and conclusion

In modern day, with increasing length of ships and its stiffening characteristics, there is a non-negligible probability of the hull girder vibration natural frequencies to be close to the range of encounter frequencies of the vessel, with respect to a typical sea spectrum. Container vessels, in general, have very low torsional rigidity due to its open deck structure. Therefore, the vessel is highly susceptible to torsional failure. The large eccentricity created between shear centre and centre of gravity causes significant coupling between torsional and horizontal modes of vibration. This changes the natural frequencies as compared to those compared to the analysis of pure horizontal vibration and pure torsional vibration. Furthermore, these vessels have thin-walled sections, and thus, warping participates significantly in the torsional vibration. Warping stiffness is a huge value as compared to St Venant’s torsional stiffness. Allowing for warping lowers the frequency of the hull significantly, causing the fundamental hull frequency to be in the range of the wave encounter frequency.

At the outset, a system of closed-form mathematical curves for semi-superellipses is used to model the hull sections. These curves helps to bypass a significant computation time for calculating various sectional properties like area, neutral axis, moment of area etc. The mathematical idealization enables the storage of the hull geometry to occupy less memory. Thus import and export of the hull geometry becomes easier as compared to NURBS surfaces. The versatility of this closed-form equation in being able to generate a wide range of body-plan shapes is shown. Their slickness in being input into the governing differential equations of vibration as closed-form expressions of the section-area properties is also seen.

Following this, the application and advantage of Rayleigh-Ritz for initial estimation of the fundamental natural frequency of the hull is demonstrated. It is conclusive that Rayleigh-Ritz offers a significant computational supremacy over the conventional FEA to study free vibration of non-uniform beam, for vertical plane vibration and for horizontal-torsion-warping coupled mode of vibration. The Rayleigh-Ritz approach provides reasonably accurate results by considering only the first few modes (say 3–5) for a highly non-uniform beam. This means we need to solve only a system of 3–5 equations as compared to a large number of equations in FEA. The accuracy has been verified by comparative studies by FEA. The free vibration (vertical, horizontal and torsion-warping) mode of vibration has been analysed and compared for various geometries (generated by rectellipses). Comparative studies are made for frequencies obtained by different analysis methodologies to provide an insight about the relative accuracies for various structural and boundary conditions assumptions. The methodology can be extended to account for shear deformation effects.

References

[1] D.-B. Li, Y.H. Chui, I. Smith, Effect of warping on torsional vibration of members with open cross-sections, J. Sound Vib. 170.2 (1994) 270–275.
[2] J.M. Pouyet, J.L. Lataillade, Torsional vibrations of a shaft with non-uniform cross section, J. Sound Vib. 76.1 (1981) 13–22.
[3] E. Dokumaci, An exact solution for coupled bending and torsion vibrations of uniform beams having single cross-sectional symmetry, J. Sound Vib. 119.3 (1987) 443–449.
[4] C. Kameswara Rao, S. Mirza, Free torsional vibrations of tapered cantilever I-beams, J. Sound Vib. 124.3 (1988) 489–496.
[5] R.E.D. Bishop, S.M. Cannon, S. Miao, On coupled bending and torsional vibration of uniform beams, J. Sound Vib. 131.3 (1989) 457–464.
[6] M. Eisenberger, Torsional vibrations of open and variable cross-section bars, Thin-Walled Struct. 28.3 (1997) 269–278.
[7] E.J. Sapountzakis, Solution of non-uniform torsion of bars by an integral equation method, Comput. Struct. 77.6 (2000) 659–667.
[8] E.J. Sapountzakis, V.G. Mokos, Non-uniform torsion of bars of variable cross section, Comput. Struct. 82.9 (2004) 703–715.
[9] Richard E.D. Bishop, William Geraint Price, Hydroelasticity of Ships, Cambridge University Press, 1979.
[10] P.T. Pedersen, Beam Theories for Torsional-bending Response of Ship Hulls, (1991).
[11] I. Senjanović, R. Grubišić, Coupled horizontal and torsional vibration of a ship hull with large hatch openings, Comp. Struct. 41.2 (1991) 213–226.
[12] Ivo Senjanović, Y. Fan, A higher-order theory of thin-walled girders with application to ship structures, Comp. Struct. 43.1 (1992) 31–52.
[13] I. Senjanović, I. Ćatipović, S. Tomašević, Coupled flexural and torsional vibrations of ship-like girders, Thin-Walled Struct. 45.12 (2007) 1002–1021.
[14] Ivo Senjanović, et al., Beam structural modelling in hydroelastic analysis of ultra large container ships, Recent Adva. Vib. Anal. (2011) InTech.
[15] Ivo Senjanović, Neven Hadžić, Nikola Vladimir, Improved methodology of ship hydroelastic analysis, Hydroelast. Mar. Technol. (2012) 115–125.
[16] N. Datta, J.D. Thekinen, A Rayleigh-Ritz based approach to characterize the vertical vibration of non-uniform hull girder, Ocean Eng. 125 (2016) 113–123.
[17] N. Datta, J.D. Thekinen, Response spectrum of non-uniform mathematical hull girder springing to deep water random seas with forward speeds, 8th International Conference in Marine Technology (2012).
[18] A.J. Sadowski, Geometric properties for the design of unusual member cross-sections in bending, Engg Structures 33.5 (2011) 1850–1854.
[19] L.S. Srinath, Advanced Mechanics of Solids, 3rd ed., Tata McGraw-Hill Education, New Delhi, 2009.
[20] S. Timoshenko, Vibration Problems in Engineering, 2nd ed., D.VanNostrand company, Inc., New York, 1937.